2003 NOAA CLIVAR/Ocean Climate Observations
Field Program on the R/V Roger Revelle
November 11 - November 26, 2003
Results from the ETL Cloud and Flux Group Measurements

C. W. Fairall, Pavlos Kollias, S. Pezoa, and Paquita Zuidema
NOAA Environmental Technology Laboratory
Boulder, CO USA

1. Background on Measurement Systems

The ETL air-sea flux and cloud group conducted measurements of fluxes and near-surface bulk meteorology during the fall field program to recover the WHOI Ocean Reference Station buoy at 20 S Latitude 85 W Longitude. The ETL flux system was installed initially in San Diego in September 2003 and brought back into full operation in Manta, Ecuador, in early November, 2003. The air-sea flux system consists of six components. (1) A fast turbulence system with ship motion corrections mounted on the jackstaff. The jackstaff sensors are: INUSA Sonic anemometer, OPHIR IR-2000 IR-hygrometer, LiCor LI-7500 fast CO2/hygrometer, and a Systron-Donner motion-pak. (2) A mean T/RH sensor in an aspirator on the jackstaff. (3) Solar and IR radiometers (Eppley pyranometers and pyrgeometer) mounted on top of a seatainer on the 02 deck. (4) A near surface sea surface temperature sensor consisting of a floating thermistor deployed off port side with outrigger. (5) A Particle Measurement Systems (PMS) Lasair-II aerosol spectrometer mounted in the same seatainer. (6) An optical rain gauges mounted on the bow tower. Slow mean data (T/RH, PIR/PSP, etc) are digitized on Campbell 21x datalogger and transmitted via RS-232 as 1-minute averages. A central data acquisition computer logs all sources of data via RS-232 digital transmission:

1. Sonic Anemometer
2. Licor CO2/H2O
3. Slow means (Campbell 23x)
4. Unused
5. OPHIR hygrometer
6. Systron-Donner Motion-Pak
7. Ship's SCS
8. ETL GPS

The 7 data sources are archived a full time resolution. At sea we run a set of programs each day for preliminary data analysis and quality control. As part of this process, we produce a quick-look ascii file that is a summary of fluxes and means. The data in this file comes from three sources: The ETL sonic anemometer (acquired at 20 Hz), the ships SCS system (acquired at 5 sec intervals), and the ETL mean measurement systems (sampled at 10 sec and averaged to 1 min). The sonic is 5 channels of data; the SCS file is 66 channels, and the ETL mean system is 42 channels. A series of programs are run that read these data files, decode them, and write daily text files at 1 min time resolution. A second set of programs reads the daily 1-min text files, time matches the three data sources, averages them to 5 or 30 minutes, computes fluxes, and writes new daily flux files. The 5-min daily flux files have been combined and rewritten as a single file

to form the file *flux_5hf_weller03.txt*. The 1-min daily ascii files are stored as *proc_nam_dayDDD.txt* (nam='pc', 'scs', or 'son'; DDD=yearday where 000 GMT January 1, 2001 =1.00). File structure is described in the original matlab files that write the data, *prt_nam_03.m*.

ETL also operated three remote systems: a Vaisala CT-25K cloud base ceilometer, a 35 GHz vertically pointed Doppler cloud radar, and a 20.6-31.65 GHz microwave radiometer. The ceilometer is a vertically pointing lidar that determines the height of cloud bottoms from time-of-flight of the backscatter return from the cloud. The time resolution is 15 seconds and the vertical resolution is 30 m. The raw backscatter profile is stored in one file and cloud base height information deduced from the instrument's internal algorithm are stored in daily files with the naming convention *CRVYYDDD.raw* where YY=03 and DDD=julian day. File structure is described in *ceilo_readme.txt*.

ETL has an integrated system in a seatainer that includes a Doppler Ka-band cloud radar (MMCR) and a microwave radiometer. The system can be used to deduce profiles of cloud droplet size, number concentration, liquid water concentration etc. in stratus clouds. If drizzle (i.e., droplets of radius greater than about 50 μm) is present in significant amounts, then the microphysical properties of the drizzle can be obtained from the first three moments of the Doppler spectrum. The radar is extremely sensitive and can detect most tropical cirrus and fair weather cumulus clouds. The Doppler capability can also be used to measure in-cloud vertical velocity statistics.

2. Selected Samples

a. Flux Data

Preliminary flux data is shown for yearday=322 November 18, 2003). The time series of ocean and air temperature is given in Fig. 1. The water temperature is about 19.2 C and the air temperature is about 18.8 C until it increases abruptly at 1230 pm GMT (730 am local) to about 19.1 C. The effect of clouds on the downward solar flux is shown in Fig. 2 and on the IR flux in Fig. 3. For the solar flux, broken clouds are apparent in the jagged form of the curve during the morning and the sharp drops in the afternoon. For IR flux, clear skies have values of about 320 Wm^{-2} and cloudy skies values around 390 Wm^{-2}. Fig. 4 shows the time series of the four of the five primary components of the surface heat balance of the ocean (solar flux is left out). The largest term is the latent heat (evaporation) flux, followed by the net IR flux (downward minus upward), the sensible heat flux, and the flux carried by precipitation. We are using the meteorological sign convention for the turbulent fluxes so all three fluxes actually cool the interface in this case. The time series of net heat flux to the ocean is shown in Fig. 5. The sum of the components in Fig. 4 is about -130 Wm^{-2}, which can be seen in the night time values; the large positive peak during the day is due to the solar flux.. The integral over the entire day gives and average flux of 166 Wm^{-2}, indicating strong warming of the ocean mixed layer

b. Remote Sensing Data

A sample ceilometer 24-hr time-height cross section for November 21 is shown in Fig. 6. This figure shows color-coded backscatter intensity with cloud base heights as black dots. This

day had 35% cloud cover and two sets of cloud base heights: the dominant stratocumulus layer with cloud bases 1000 to 1200 m and occasional lower level 'scud' clouds with bases about 500 m. Small amounts of drizzle can be seen as the light blue color right below cloud base (e.g., 1430 GMT at 500 m). A sample time-height cross section (Fig. 7) from the cloud radar is shown for a 24-hr period on November 18. The panels indicated the intensity of the return (upper), the mean fall velocity of the scattering droplets (middle panel), and the Doppler width of the return. This happens to be a day with low cloud cover; clouds are fairly thin with tops at 1.0 - 1.2 km. Light drizzle events are apparent as the 0830 and 1430; the radar is much more sensitive to drizzle than the ceilometer.

3. Cruise Summary Results

a. Basic Time Series

The 5-m time resolution time series for sea/air temperature are shown in Fig. 8 and for wind speed and N/E components in Fig.9. The change in conditions for the first three days of the record is associated with the run south from Manta, Ecuador, to the WHOI buoy at 20 S. Time series for flux quantities are shown as daily averages. Fig. 10 gives the flux components and Fig. 11 the net heat flux to the ocean. The diurnal cycle of cloudiness at 20 S shows up as the larger values of net heat flux and solar flux at 20 S where afternoon clearing leads to much greater 24-hr average solar flux. Just for amusement, the transect from 85 W to 75 W along 85 S is shown in Fig. 12. The diurnal cycle appears to be much stronger than longitudinal variations.

b. Boundary Layer and Cloud Properties

Beginning on November 14 and ending on November 24 we completed 45 successful rawinsonde launches (4 times daily at 0, 6, 12, and 18 UTC). A time-height color contour plot of temperature is shown in the upper panel of Fig. 13; the middle panelshows the relative humidity and winds (zonal and meridional; these use the meteorological convention, with northerly, easterly, southerly, and westerly winds shown as arrows pointing 0, 90, 180, and 270 degrees counter-clockwise from north).
The boat was in transit from Manta from Julian day (JD) 318 until 319.5, and stationary thereafter at the WHOI buoy from JD 319.5 until JD 325.5.

A pronounced temperature inversion is evident at approximately 1.0-1.5 km. On JD 323 the inversion is less pronounced. The boundary layer below the temperature inversion has relative humidity consistently above 65%, and drizzling episodes are marked by relative humidity above 90 %. Two time periods with relative humidity above 90% occur at the surface; these correspond with drizzle detectable by surface observers on the Revelle. The winds are consistent with climatology, with southeasterlies prevailing within the boundary layer and westerlies aloft.

An interesting aspect of Fig. 13 is two episodes of higher relative humidity subsiding from aloft into the boundary layer. The more pronounced case occurs on JD 322-324 (Nov. 18-20), and another, drier, example occurs from JD 318-321 (Nov. 14-17). In both cases the depth of the boundary layer moisture increases when the subsiding moisture slug reaches the boundary layer, and corresponds with drizzling time periods evident within the cloud radar data. For the

second case, cloud tops appear to reach 1.4 km on Nov. 19, coinciding with the weakest temperature inversion measured during the cruise.

The bottom panel of Fig. 13 shows the virtual potential temperature (θ_v)as calculated from the rawinsonde data, along with the lifting condensation level (LCL) of an air parcel with the mean temperature and relative humidity of the 1000-1010 mb layer (an approximately 100 m thick air layer slightly above the ocean surface). θ_v provides a measure of the air buoyancy; lower values indicate air that is less able to rise. θ_v is a conserved quantity within a moist, well-mixed air layer, independent of whether the moisture is gaseous or liquid. Nevertheless, a strong variability is evident within the boundary layer. Low values often correspond to the cooling associated with the evaporation of drizzle. This cooling will tend to inhibit further stratus/stratocumulus cloud development, by discouraging the moisture flux from the surface necessary for the cloud maintenance.

The lifting condensation level corresponds well with the ceilometer-derived cloud base (Fig. 14) and also demonstrates a strong variability. During drizzling episodes, the LCL is lowered by the high moisture content of the lower boundary layer, for example towards the end of JD 323. The time series of data from the microwave radiometer is shown in Fig. 15. The period from 318-322 was clearly drier (vapor = 1 cm) than 323-328 (vapor = 2 cm). There does not to be any correlation with total column vapor and liquid water. Days 322-323 (November 18-29) were the most cloud free.

Data from the PMS Lasair-II aerosol spectrometer is shown in Fig. 16. This instrument counts particles in size ranges from 0.1 to 5 μm diameter based on scattering of light from a laser beam. This size range includes most of the so-called accumulation-mode aerosols that represent most of the particles activated to form droplets in clouds. Thus, the total number of aerosols counted by this device is expected to correlation with cloud condensation nuclei and the number of cloud drops. More detailed aerosol information was obtained by Jason Tomlison (Texas A&M University). The Lasair-II time series shows periods of significant reductions in particles (from 200-300 to 20-30) on days 320 (November 16), 323 (November 19), and late 325 – early 326 ((November 21-22). These were also the days with decoupled boundary layers (as indicated by scattered clouds below the main stratus deck) and significant drizzle.

Data from the cloud radar, ceilometer, and rawinsonde system have been processed and combined in Fig. 17 to display cloud boundaries. Cloud top is determined from an intensity threshold on the radar backscatter signal. Cloud base is directly from the ceilometer algorithm. Lifting condensation level (LCL) is computed from the lower part of the sounding (as in Fig. 13). Co-location of the LCL and ceilometer cloud base implies a well mixed atmospheric boundary layer.

4. ETL Data Cruise Archive

Selected data products and some raw data were made available at the end of the cruise for the joint cruise archive. Some systems (radar, turbulence, microwave radiometer) generate to too extravagantly to be practical to share. Compared to processed information, the raw data is of little use for most people. For the radar we have made available image files only. For the microwave radiometer, the time series after some processing and averaging. No direct turbulent flux information is provided; that will be available after processing is done back in Boulder. However, bulk fluxes are available in the flux summary file.

Data Archive Directories

Ceilo	Ceilometer files (processed file, images)
Flux	Air-sea flux files (processed flux files: daily files, cruise file, some m-files)
Rawship	The entire Revelle ship data file at 5 s resolution as logged by ETL
Ship	ETL processed files from the Revelle system
Ballones	Rawindsone files (.PTU and .WIND)
Microwv	Microwave radiometer files (processed files; graphic display)
Radar	Image files from cloud radar
Aerosol	Lasair II (particle count file; graphic file)
Reports	Documentation (cruise report, school writeup, summary image files)

Contact:
C. Fairall
NOAA Environmental Technology Laboratory
325 Broadway
Boulder, CO USA
303-497-3253
chris.fairall@noaa.gov

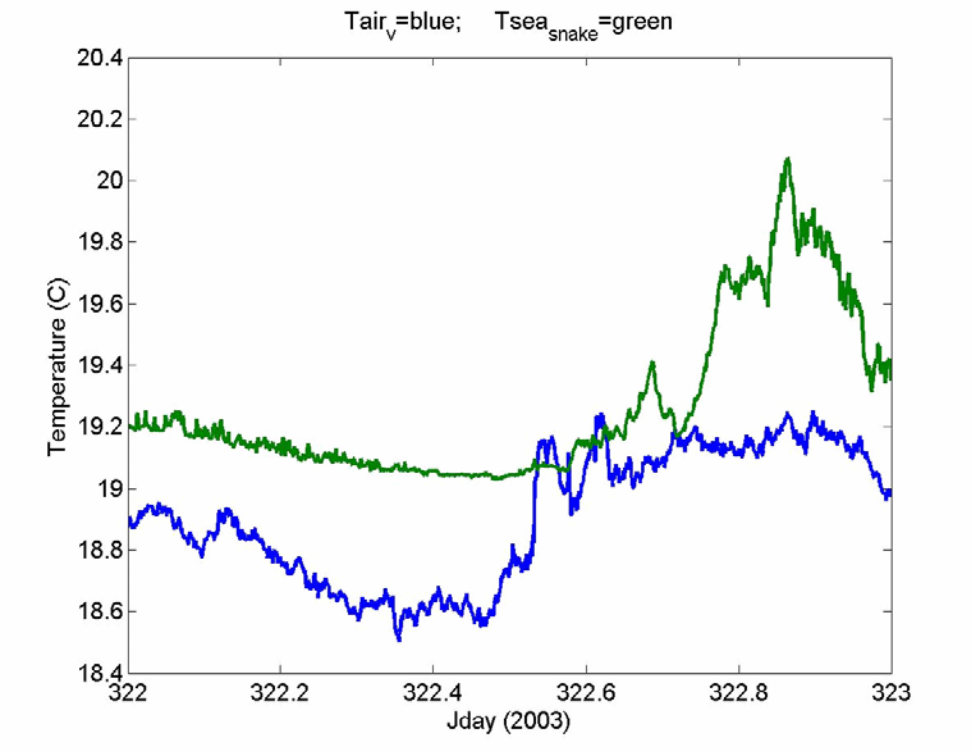

Figure 1. Time series of near-surface ocean temperature and 18-m air temperature

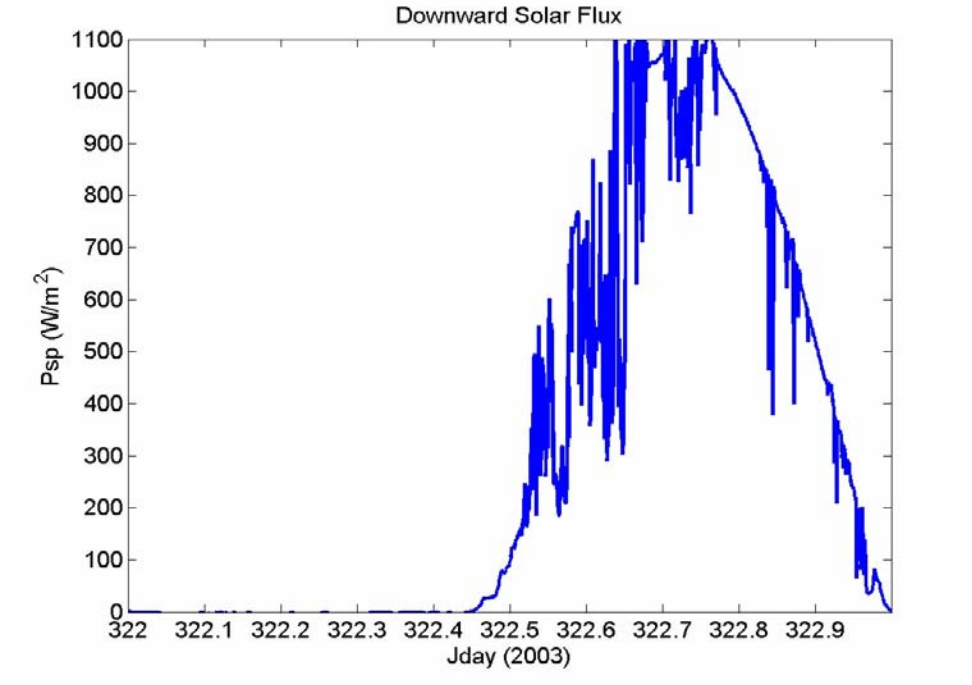

Figure 2. Time series of downward solar flux.

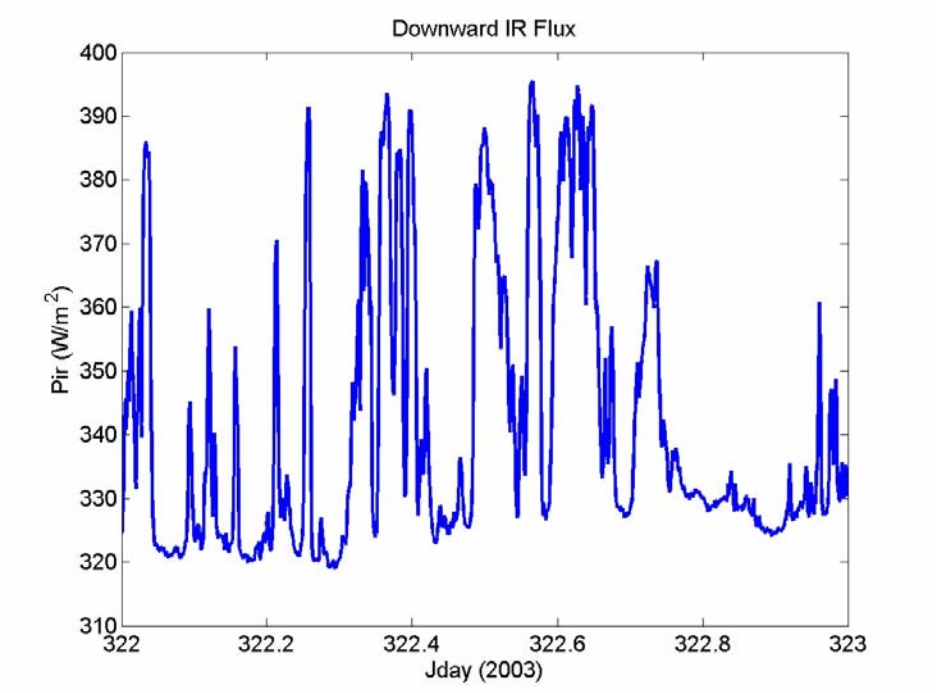

Figure 3. Time series of downward IR flux.

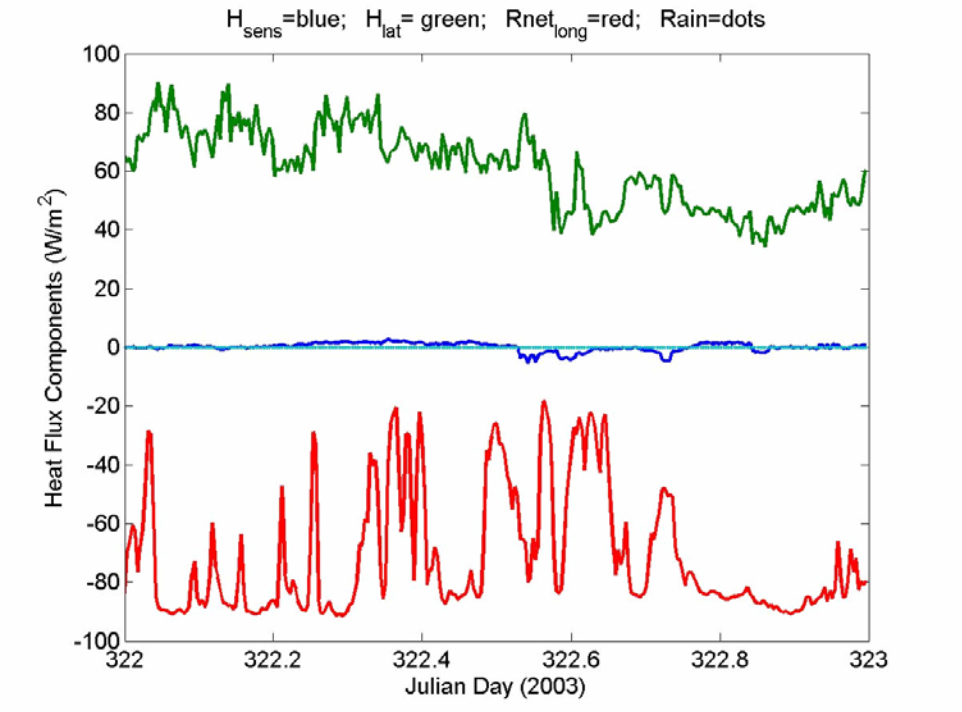

Figure 4. Time series of surface heat flux components: sensible (blue), latent (green), and net IR (red)

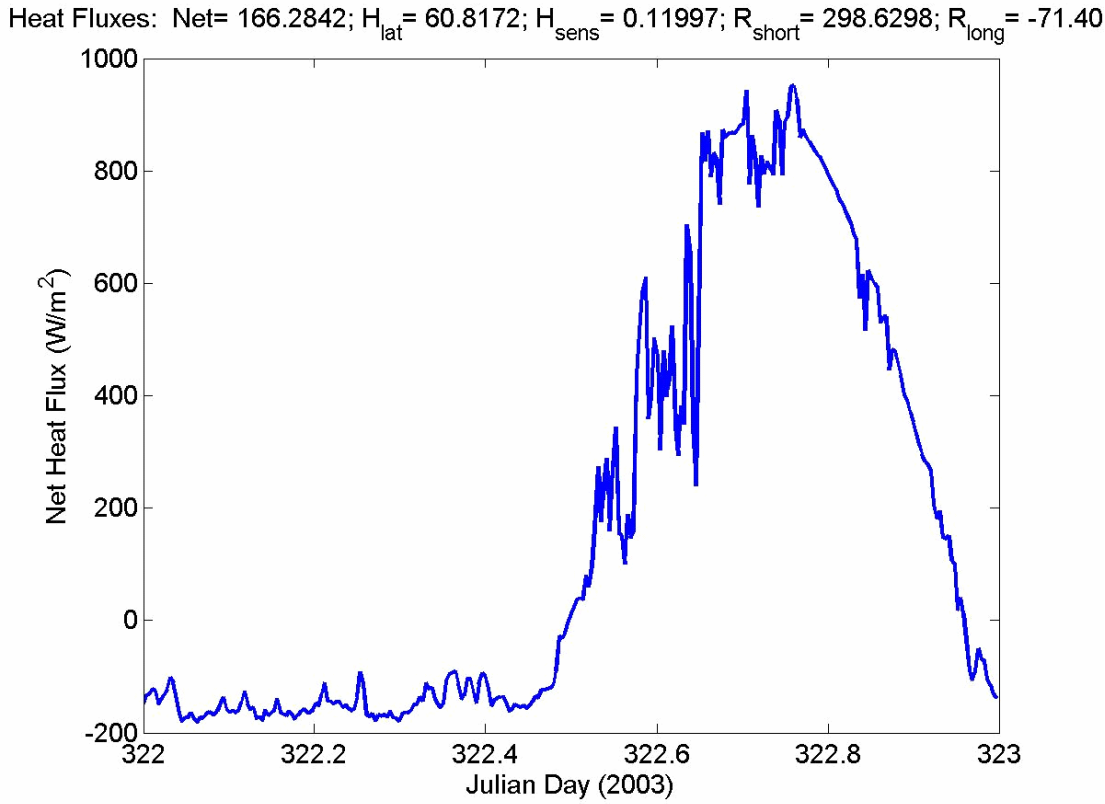

Figure 5. Time series of net heat flux to the ocean surface. The values at the top of the graph are the average for the day.

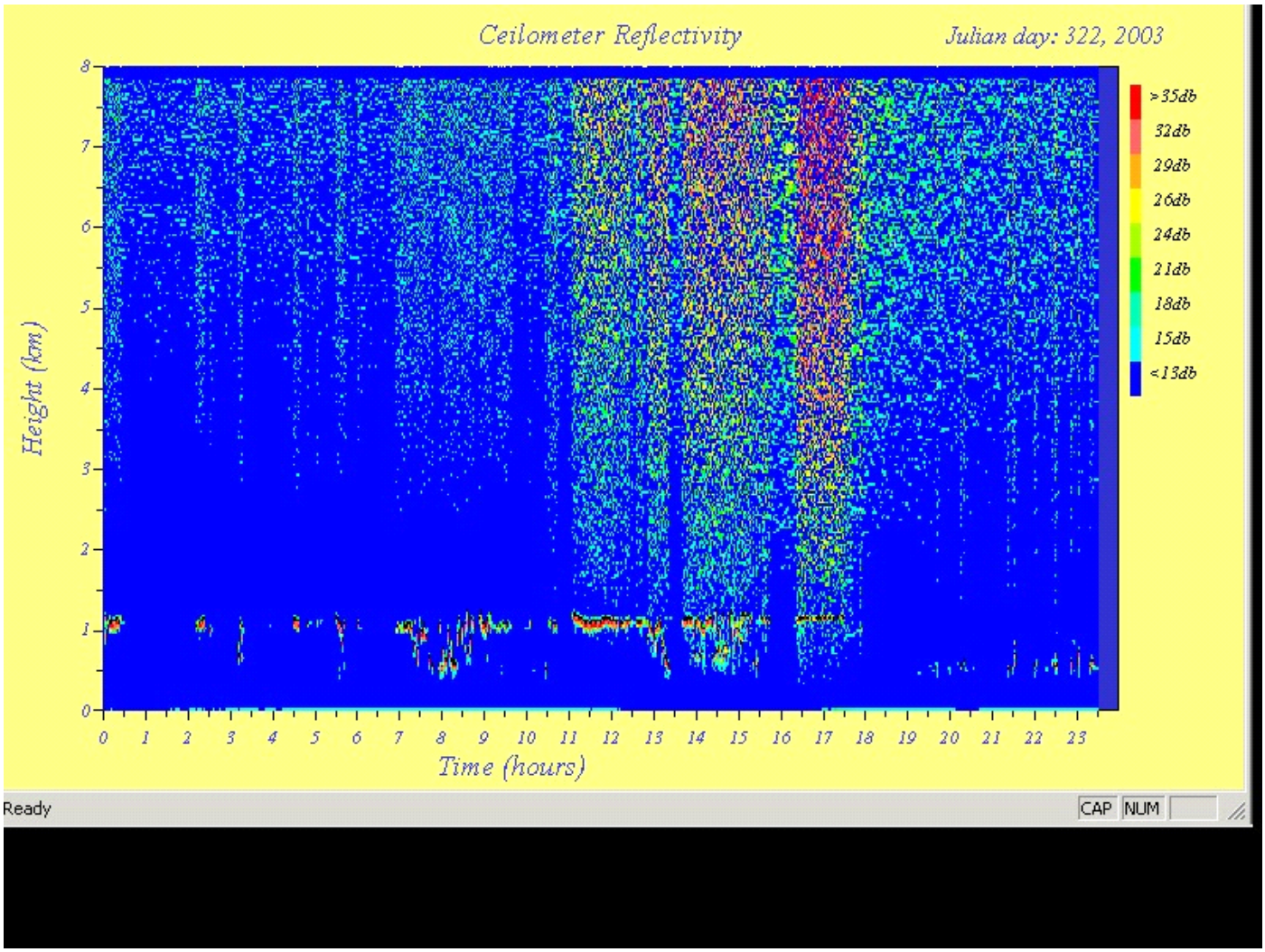

Figure 6. Time height cross-section of low cloud base data for day 322 (November 18, 2003). The colors denote the intensity of the lidar return; the black dots are the cloud base height at that time. The speckled color regions above the clouds are noise caused by diffuse sunlight.

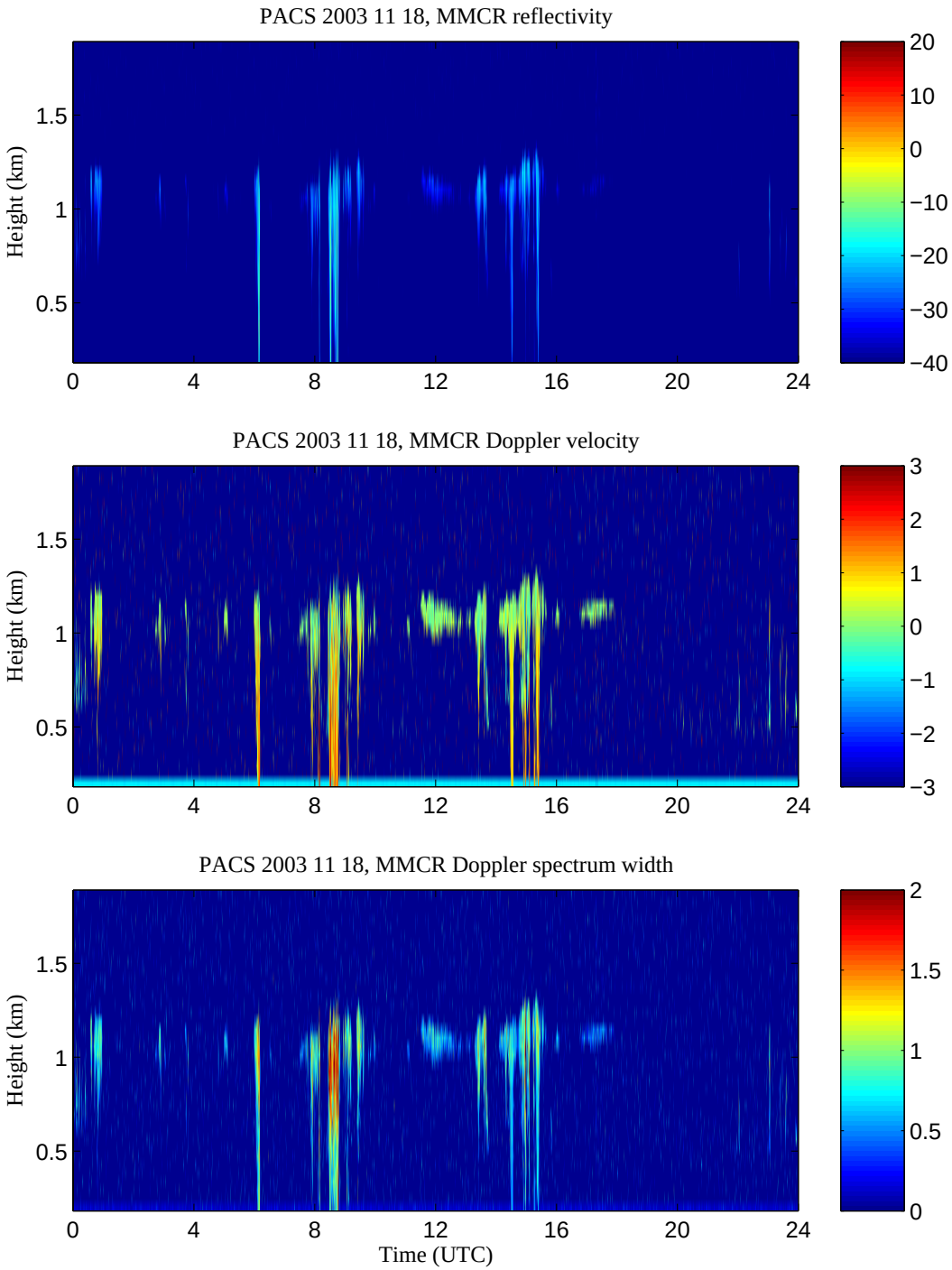

Figure 7. Time-height cross section data from 35 GHz cloud radar: backscatter intensity (upper panel), mean Doppler fall velocity (middle panel), and Doppler spectrum width (lower panel).

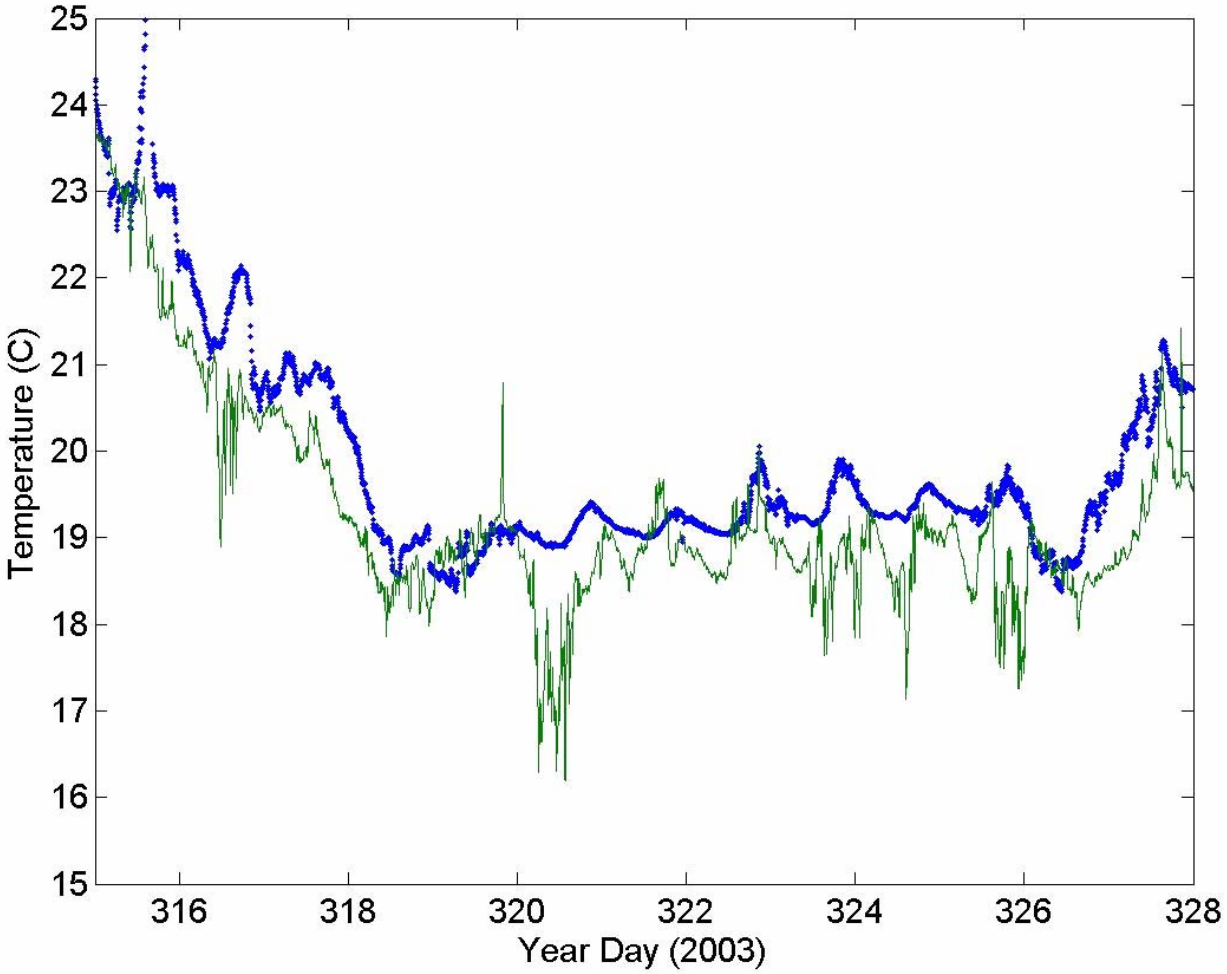

Figure 8. Time series of near-surface ocean temperature and 18-m air temperature for the 2003 Revelle cruise.

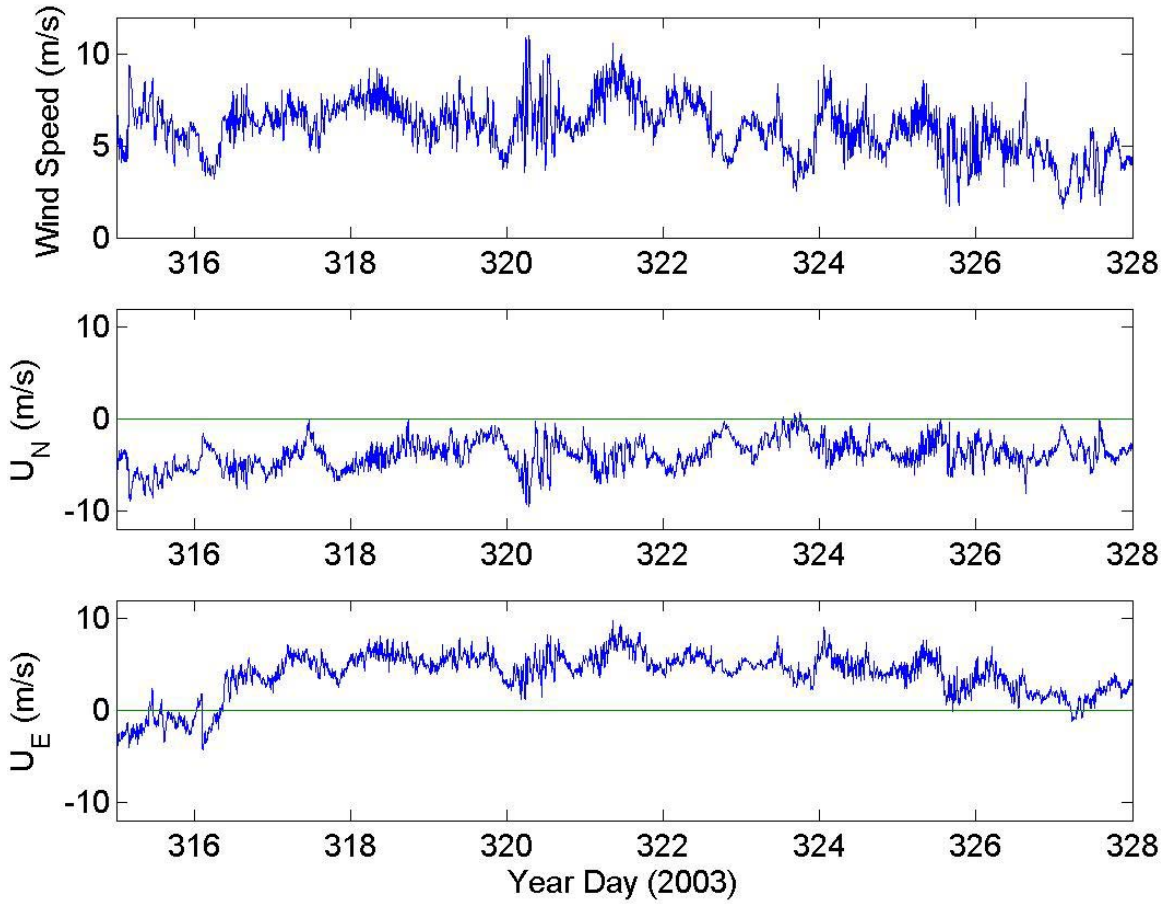

Figure 9. Time series of wind speed (upper panel), northerly component (middle panel), and easterly component (lower panel) for the 2003 Revelle cruise.

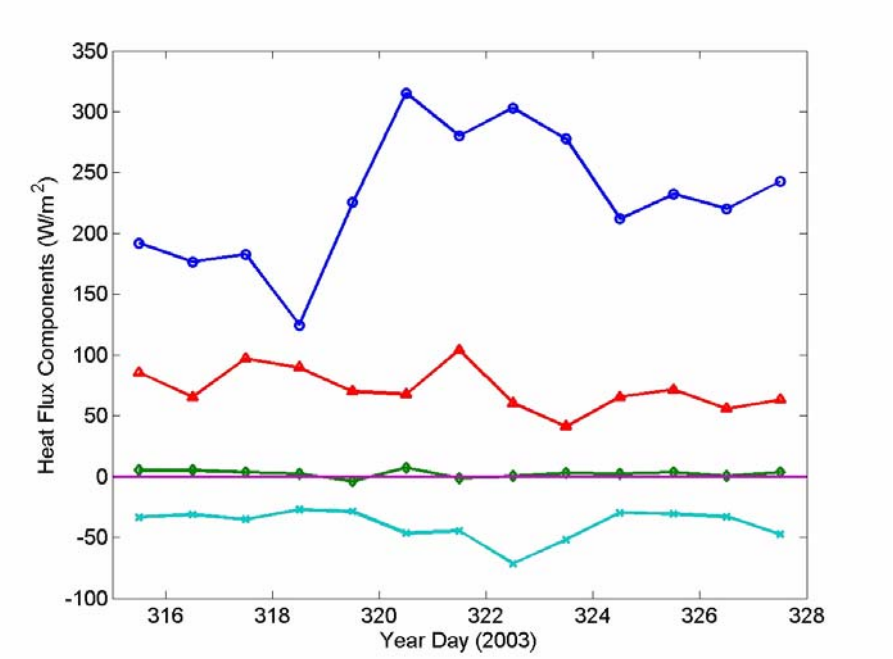

Figure 10. Time series of 24-hr average heat flux components: solar flux - circles; latent heat flux - triangles; sensible heat flux - diamonds; net IR flux x's.

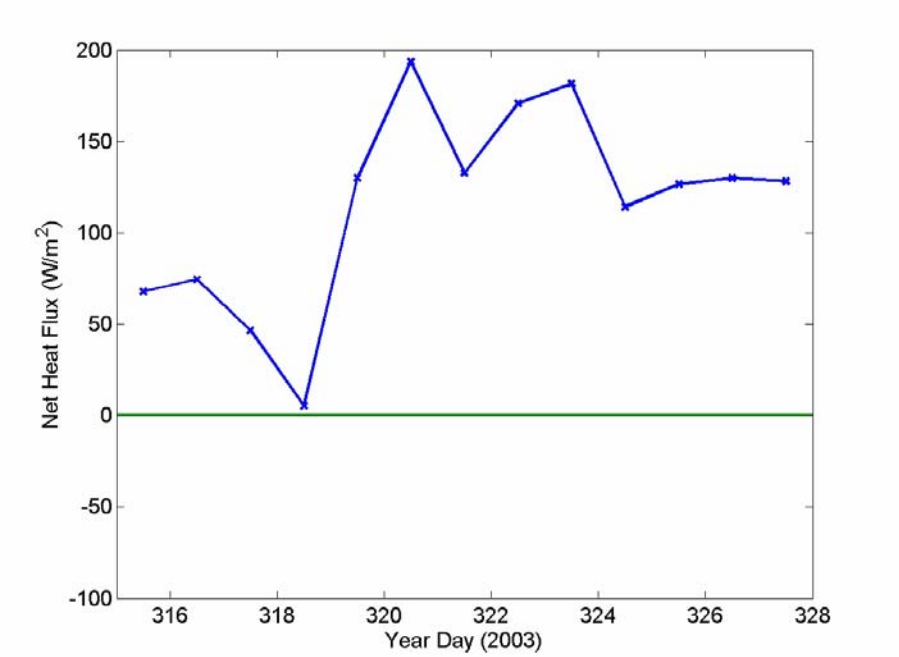

Figure 11. Time series of 24-hr average net heat flux to the ocean.

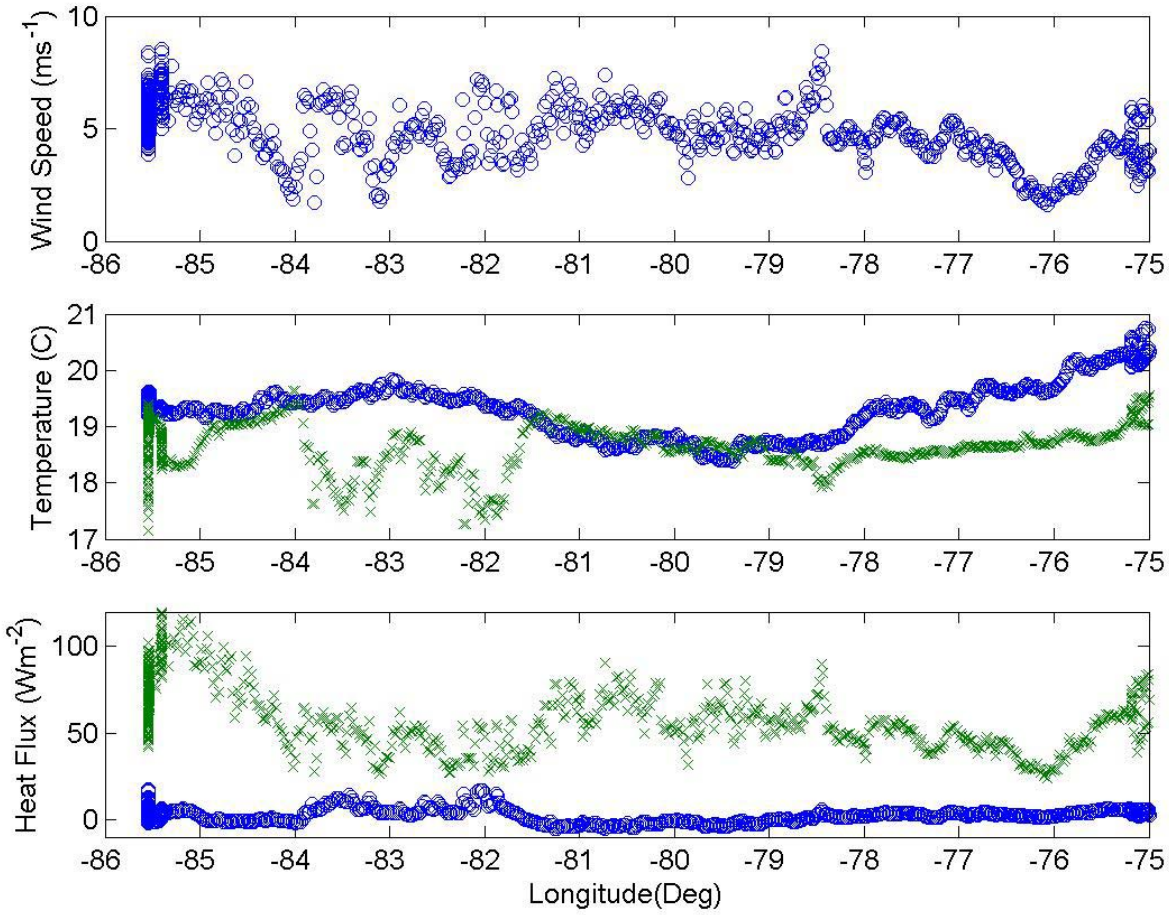

Figure 12. Meteorological variables as a function of longitude from the WHOI buoy position (85 W) to the DART buoy position (75 W): upper panel - wind speed; middle panel ocean near-surface temperature (circles) and air 18-m temperature (x's); lower panel sensible heat flux (circles) and latent heat flux (x's).

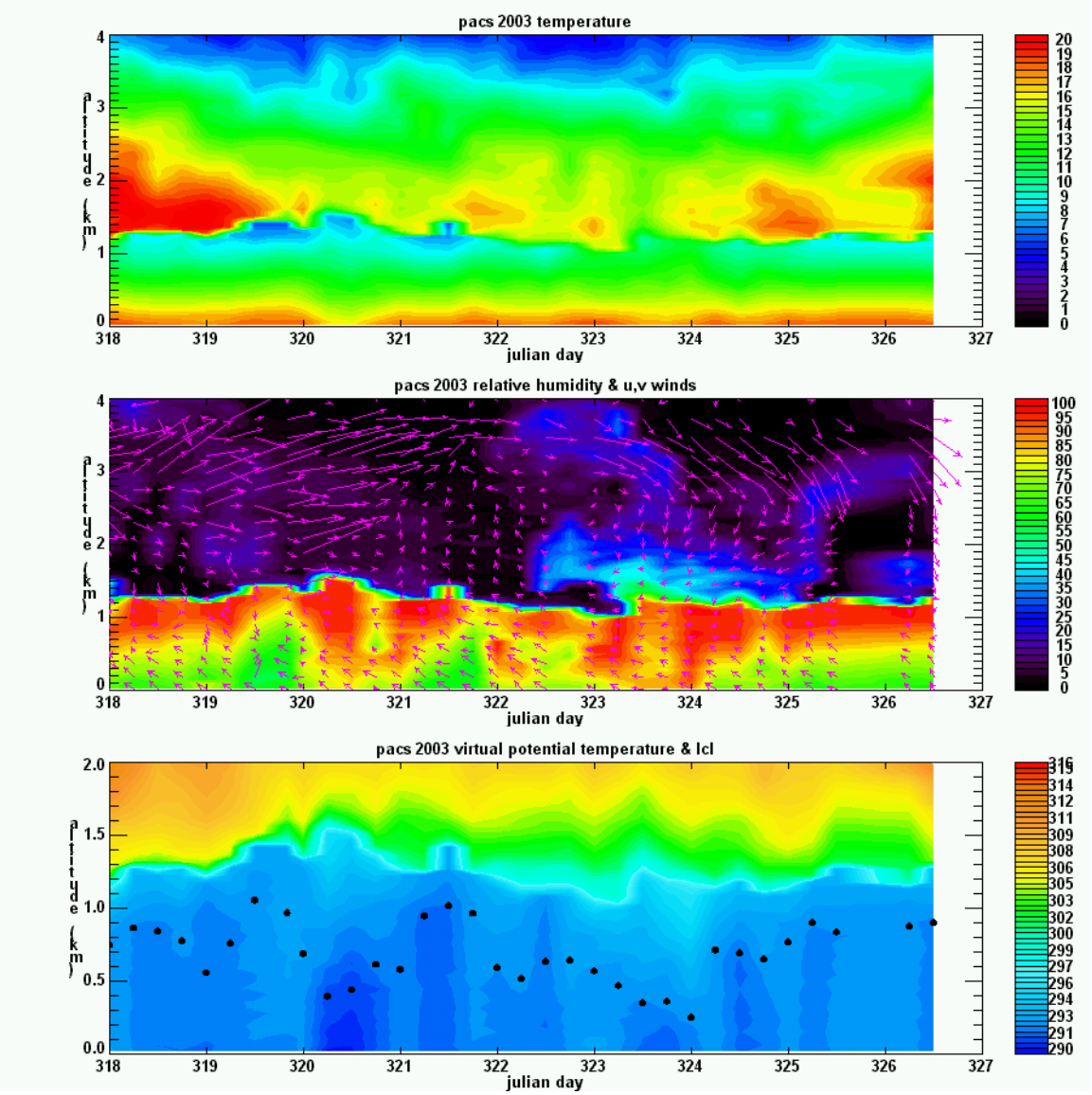

Figure 13. Time-height color contour plots from rawinsondes launched during the 2003 Revelle cruise. The upper panel is temperature. The middle panel is relative humidity with arrows depicting the horizontal wind (vertical is to the north, etc). The bottom panel is virtual potential temperature; the black dots are the lifting condensation level computed from the lower part of the profile.

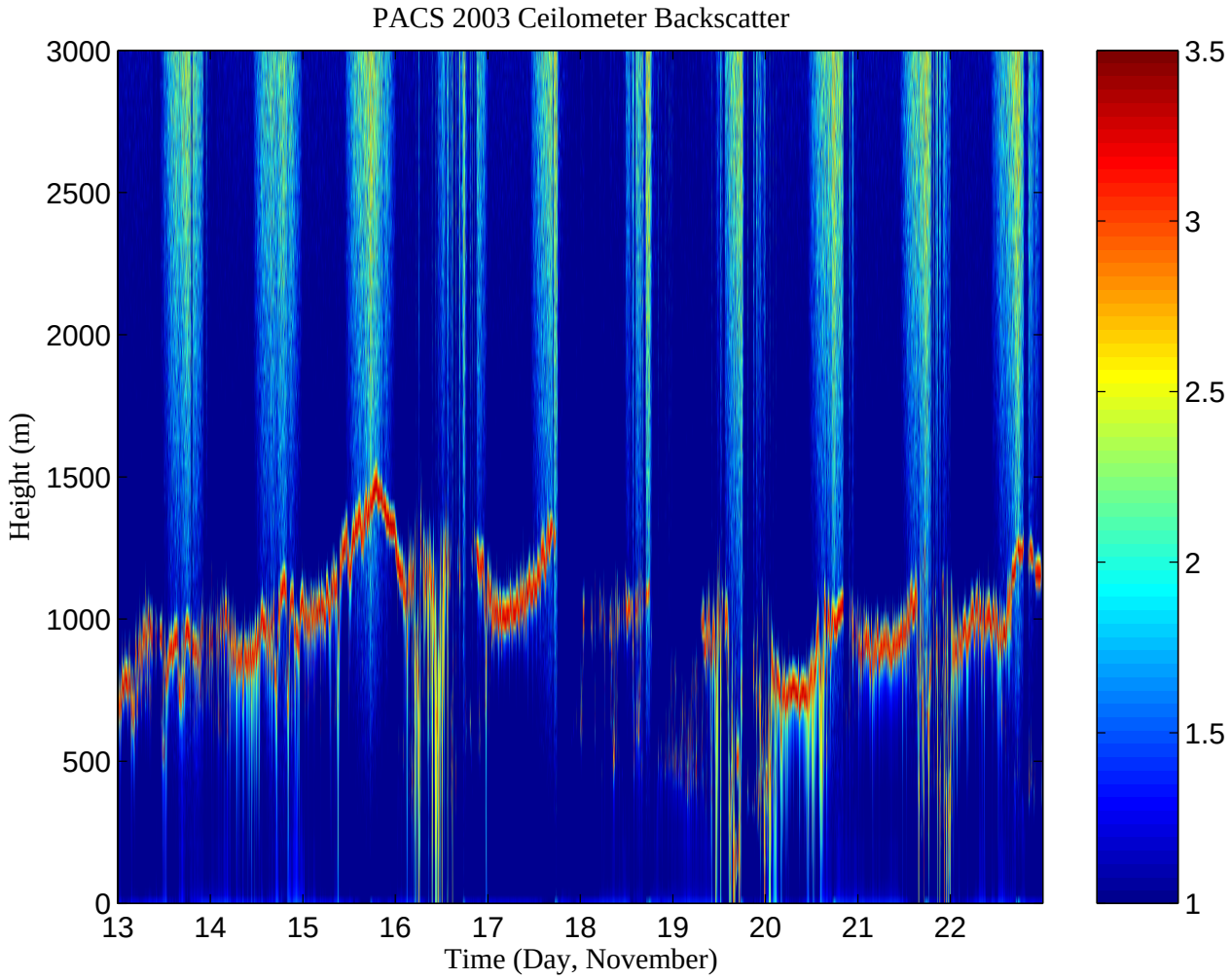

Figure 84. Time-height cross section for the ceilometer backscatter intensity for the entire experiment. Cloud base is near the maximum intensity region (red color).

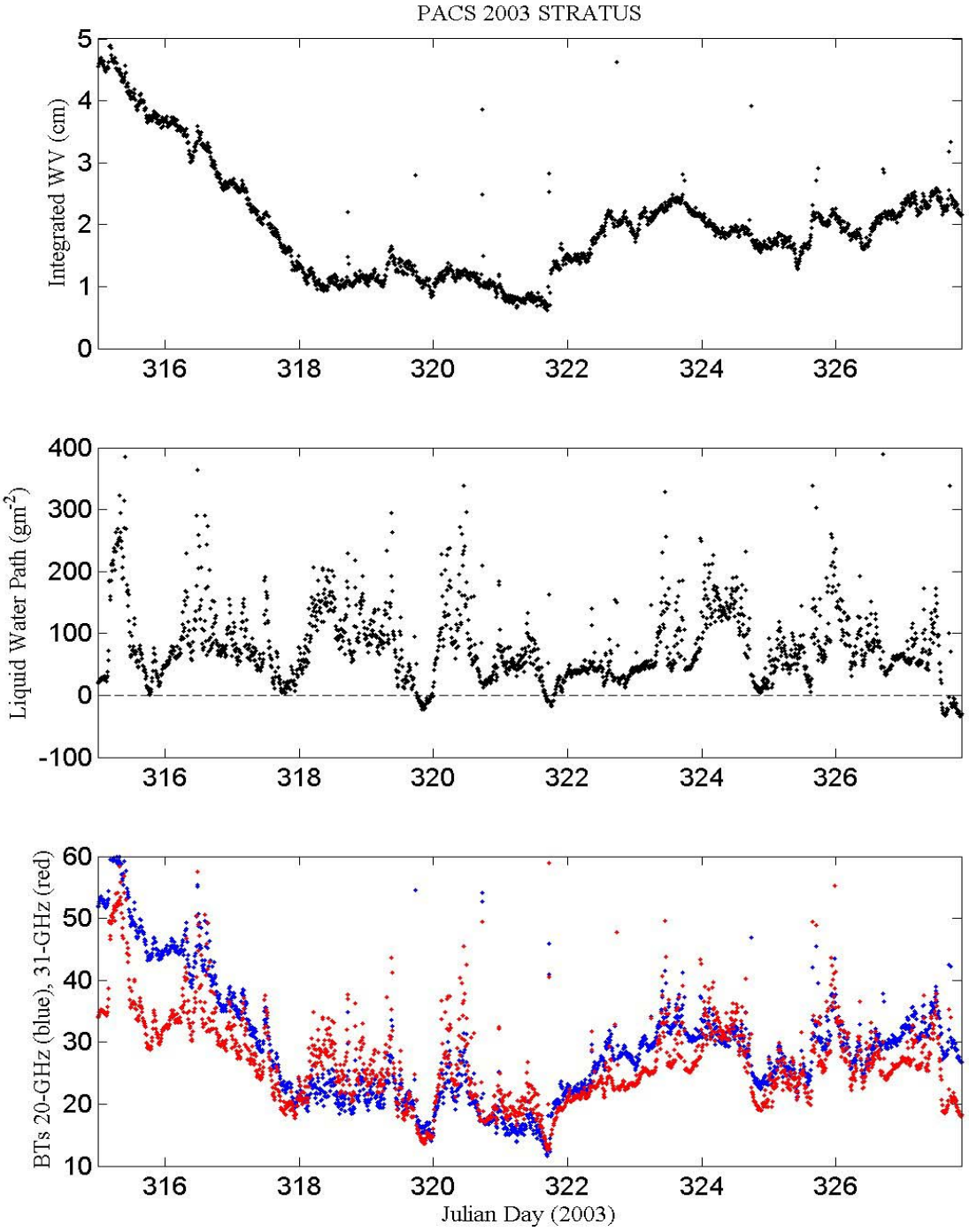

Figure 15. Time series of data from the 21-31 GHz microwave radiometer at 10-min resolution: column water vapor (upper panel), column liquid water path (middle path), and microwave brightness temperature (bottom panel) at 20.6 GHz (blue) and 31.65 GHz (red).

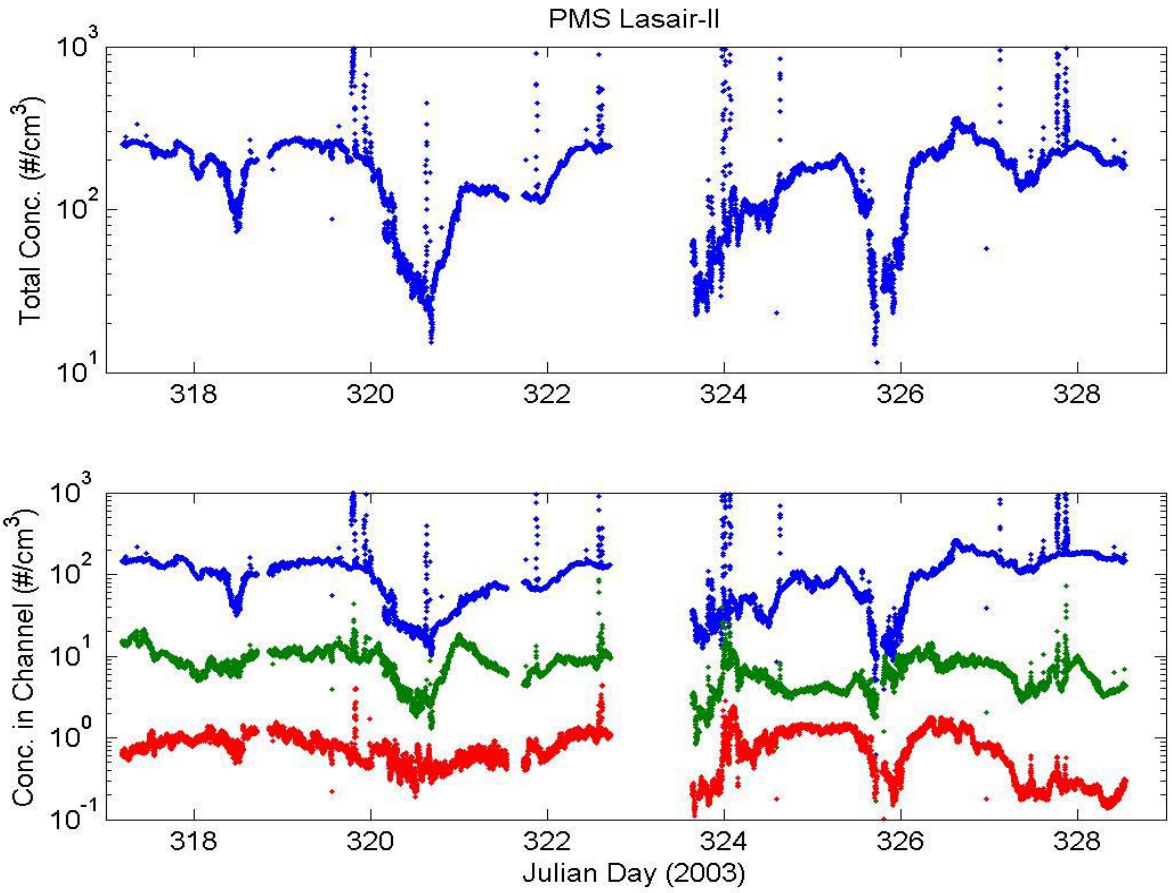

Figure 16. Aerosol data from the ETL PMS Lasair-II size spectrometer. The upper panel shows concentration for sizes greater than 0.1 µm diameter. The lower panel shows concentrations for channels 0 (0.1 – 0.2 µm) , channel 2 (0.3 – 0.4 µm), and channel 4 (1 – 5 µm). The large positive spikes are caused by encounters with the ship's exhaust plume.

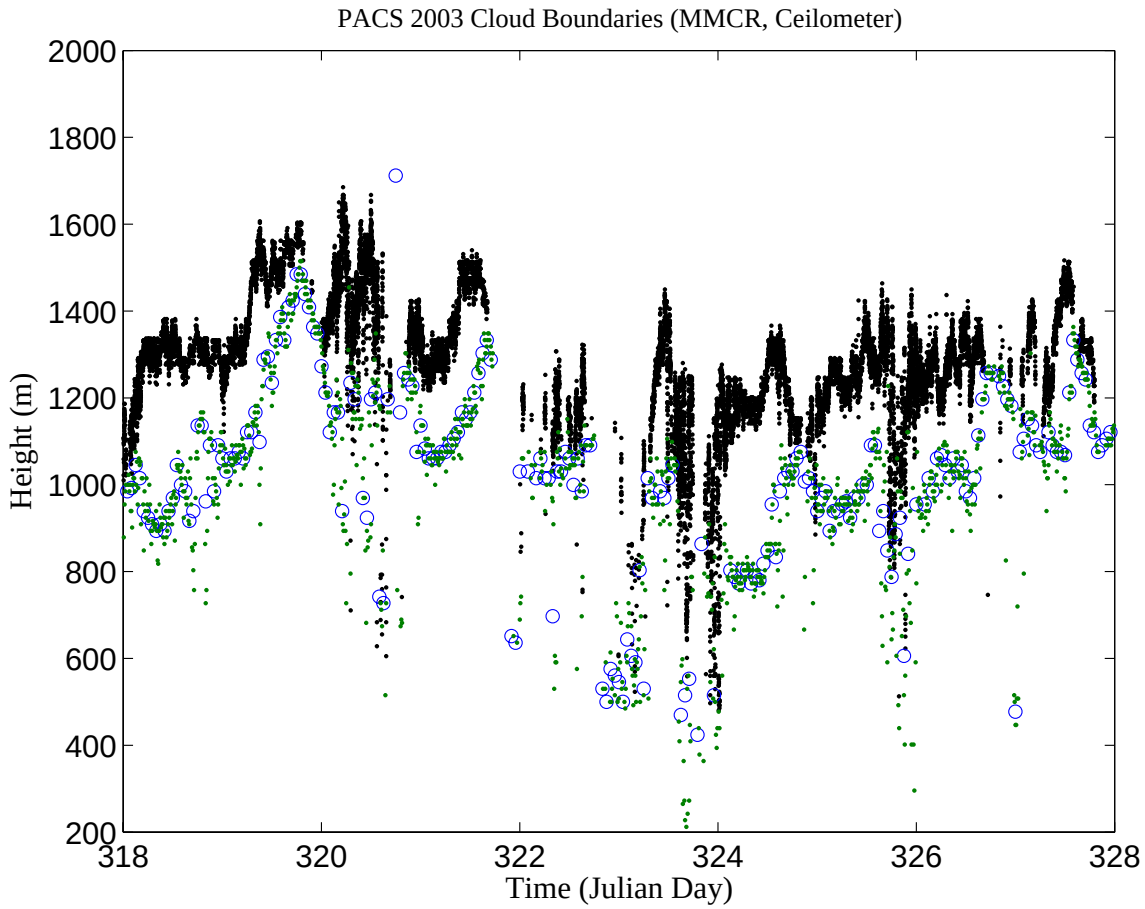

Figure 17. Time series of cloud top height (black dots) from the radar and cloud base height (green dots) from the ceilometer. The blue circles are lifting condensation level (LCL) from the rawinsonde temperature and humidity data. LCL is a thermodynamic estimate of cloud base for a well mixed boundary layer.